Sensors and Actuators A 217 (2014) 139–150

Contents lists available at ScienceDirect

Sensors and Actuators A: Physical

journal homepage: www.elsevier.com/locate/sna

Long-term testing of a vibration harvesting system for the structural health monitoring of bridges

J.J. McCullagh*, T. Galchev, R.L. Peterson, R. Gordenker, Y. Zhang, J. Lynch, K. Najafi

Department of Electrical Engineering, Center for Wireless Integrated MicroSensing and Systems (WIMS²), University of Michigan, EECS Building, 1301 Beal Ave., Ann Arbor, MI 48109-2122, USA

ARTICLE INFO

Article history:
Received 14 October 2013
Received in revised form 2 July 2014
Accepted 7 July 2014
Available online 17 July 2014

Keywords:
Frequency up-conversion
PFIG
Vibration harvesting
Structural health monitoring
Wireless sensors
Charge pump

ABSTRACT

Advances in energy harvesting systems are needed to power wireless sensors for structural health monitoring. Research on developing a harvesting system that converts the low frequency, non-periodic, and low-acceleration vibrations present on bridges is continued and significantly extended in this work. The mechanics of the harvester were optimized to increase its robustness and lifetime, power electronics were added, and the complete system was installed on the New Carquinez suspension bridge in California. The complete results and analysis are presented in this study. The power management circuit is added to rectify and boost the low AC output of the harvester and convert it into a usable DC voltage. The harvester design is further enhanced to significantly improve performance and robustness. During short-term on-bridge testing, the system was able to charge a 10 μF capacitor to 2 V DC, and the average harvester output power ranges from 1.6 to 5.0 μW, depending on the location on the bridge, a 10× improvement over previous results. A long-term test of the harvesting system has been conducted, during which the performance of the system was monitored remotely using a wireless sensor network. The system improvements described in this study enabled continuous operation in the harsh bridge environment for 13 months starting April 30, 2012 and constitute a major milestone in the development of miniaturized motion harvesters. Finally, the system was retrieved and analyzed to understand and verify the cause of observed long-term performance changes.

1. Introduction

According to the US Department of Transportation, a significant fraction of the nation's bridges are rated as structurally deficient or functionally obsolete [1]. Wireless sensor technology is a superior solution for monitoring aging infrastructure systems (such as bridges) as it eliminates the need for expensive wiring and permits easy relocation of sensors nodes. As these Structural Health Monitoring sensors (SHM) must operate continuously for many years without human intervention, battery replacement is a significant concern since the sensors are typically located in hard-to-reach and dangerous locations. Hence, the ability to harvest power near the sensor for storage in a local rechargeable cell is desirable. The New Carquinez Bridge near Vallejo, California (also known as the Alfred Zampa Memorial Bridge) (Fig. 1), where this study was completed, is an example of a large suspension bridge over water with heavy traffic containing many such inaccessible locations.

There are multiple energy sources that can be utilized on a bridge, including solar, thermal, radio frequency (RF), and mechanical energy. Each of these methods has benefits and drawbacks. Solar energy is presently being used to power SHM nodes on bridges, including the previously mentioned New Carquinez Bridge [2]. Solar panels produce sufficient power on sunny days for regular sensor data collection and transmission, but power is limited or non-existent during the night, cloudy periods, or when excessive dust accumulates on the solar panels. For SHM nodes at interior points or under the bridge deck, wiring must be routed from the solar panels on the bridge surface to the sensor locations, adding significantly to the system complexity and cost. Thermal harvesting from the temperature difference between the bridge surface and the outside air has been investigated and shows promise [3]; however, the available temperature difference varies and can be very small, making reliable harvesting a challenge. RF harvesting also has been investigated [4]; however, little RF power is typically available in the environment due to the rapid attenuation away from distant transmitters. Solutions using dedicated RF transmitters in close proximity to or on the bridge can supply considerably more power to the RF harvesters [3]; however, their installation

* Corresponding author. Tel.: +1 734 763 2126.
E-mail address: jamesjmc@umich.edu (J.J. McCullagh).

http://dx.doi.org/10.1016/j.sna.2014.07.003
0924-4247/

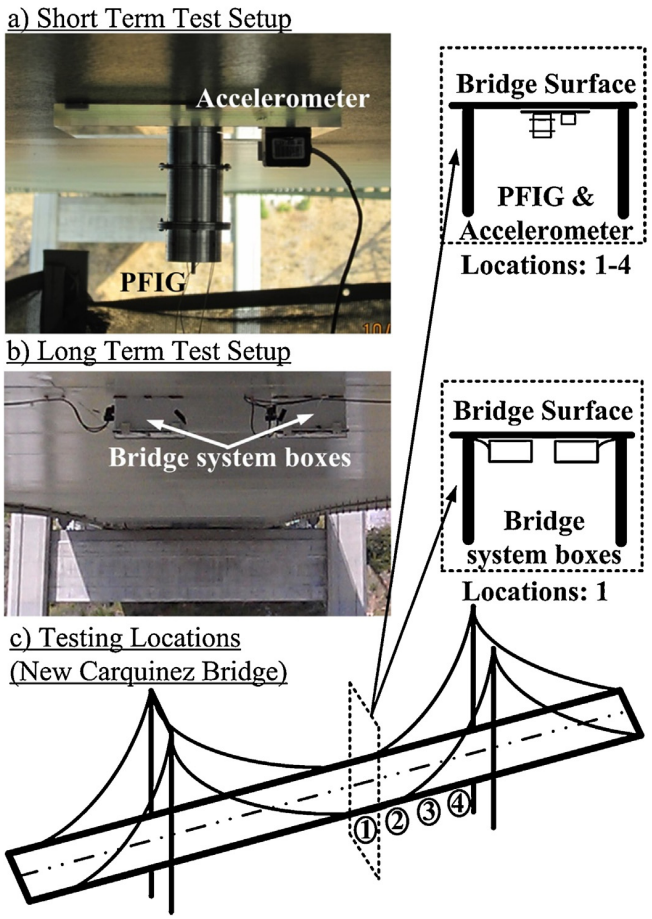

Fig. 1. (a) Short-term test setup with the PFIG and accelerometer. The PFIG is attached to a plastic plate attached magnetically to the bottom of the bridge. (b) Long-term test setup is shown with system boxes attached magnetically to the bottom of the bridge. (c) Approximate positions of installation locations the New Carquinez Bridge. Locations 1–4 were used for short term tests, while the location 1 was used for long term tests [32].

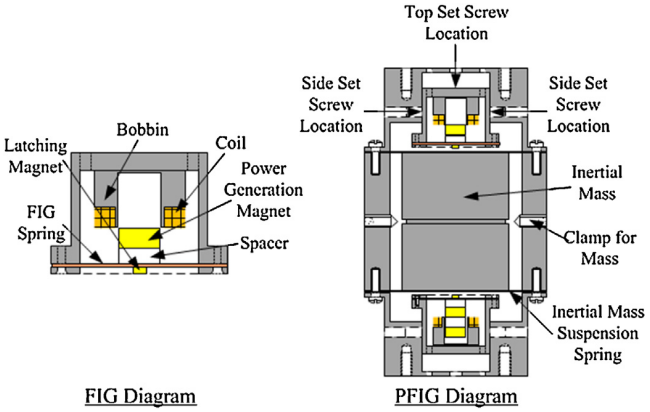

Fig. 2. A schematic of the PFIG design installed on the bridge for long term testing.

may not always be feasible. While each of these harvesting methods has certain advantages, none of them alone supplies the continuous energy needed to power wireless sensors throughout the bridge. This motivates the need to investigate other sources of long-term renewable energy such as vibrations, which are the focus of this paper. While a few harvesters have been tested on various bridges [5–8], none have been investigated over long periods of deployment to assess their long-term performance.

Vibration energy harvesting may be an effective way to power wireless SHM sensors by harvesting power during periods of high traffic and storing that power for later use. Resonant vibration harvesters for powering a bridge SHM sensor [6–8] have been demonstrated, where the resonant frequency of the harvester was tuned to a modal frequency of the bridge at the specific sensor location to obtain optimal performance, and a system [6] has even been tested for one week. Studies show that bridge resonant frequencies can vary significantly from bridge to bridge or between positions on the bridge [3], so it may be difficult to broadly apply resonant harvesters. A number of tuning approaches that automatically [9,10] vary the harvester resonant frequency and adjust it to maximize energy will not work in this case because they consume too much power and vibration characteristics vary spatially on the bridge as well as over time.

Previously the non-resonant, broadband Parametric Frequency Increased Generator (PFIG) was introduced, based on the principle of mechanical up-conversion [11]. Multiple versions of the PFIG have been published including a bench-top version [12] and smaller self-contained piezoelectric and electromagnetic versions [13,14]. In the last publication a PFIG for bridge SHM was introduced (PFIG-B1) [5]. It converts the non-periodic, low-acceleration, and low-frequency bridge vibrations into higher-frequency mechanical oscillations that can be electrically transduced and finally converted to a DC voltage. The device was shown to operate on multiple bridge locations nearly identically without the necessity to tune or modify it in-between installations. The PFIG (shown in Fig. 2) consists of a large inertial mass which snaps back and forth between latching magnets on the springs of two electromagnetic transducers, referred to here as FIGs [5,12–15]. The inertial mass is actuated when the bridge motion externally displaces the PFIG casing. The latch and release operation transfers energy from the inertial mass to the FIG. The FIG springs vibrate at an up-converted frequency (~130 Hz) and displace attached magnets, thereby creating a variable field that induces voltage in stationary coils surrounding the magnets. The entire volume of the PFIG-B1 is minimized to be about the size of a "D" cell battery (<68 cm^3). The technical viability and in situ characterization of the PFIG-B1 was completed during a temporary installation on the New Carquinez Bridge (Fig. 1a). The measured average output power was 0.5–0.75 μW over several minutes, when bridge accelerations ranged from 0.1–0.5 m/s^2 at frequencies of 2–30 Hz [5].

In addition to the electromechanical behavior of the harvester, power management and rectification is essential at the system design level. Essential elements in vibration harvesting typically involve AC to DC conversion, voltage boosting, and regulation. In the case of the PFIG-B1 harvester a number of challenges exist that make these power management tasks complicated. First the electrical outputs of the PFIG resemble decaying sinusoidal waveforms due to the nature of the up-conversion process. Second, the PFIG-B1 harvester has a high output impedance (1.5 kΩ). Lastly, the harvester produced a non-optimized low output voltage [5]. A preliminary attempt at power management was made by using two cascaded six-stage passive Schottky diode charge pumps to simultaneously rectify and boost the PFIG output signal [5]. However, this circuit exhibited a very low efficiency (simulated 13% with a decaying sine wave input of peak 375 mV), and ceased to work below 200 mV. The main problem was the low output voltage relative to the turn-on voltage of the Schottky diodes.

Many AC–DC converters have been proposed for use in vibration harvesting including active rectifiers, boost rectifiers, and both passive and active charge pumps. One can use active rectifiers

[16–21]; however, start-up issues have to be addressed, and more importantly they have poor efficiency when the inputs and rectifier supply are below the threshold voltage of typical MOSFETS ~400 mV. LC-boost or integrated switched capacitor charge pumps rectifiers are other alternatives, but these two types of AC–DC converters need ancillary clocking circuits, a start-up charge pump [22], a pre-charged battery [23] or high voltage inputs (≥~0.8 V) to enable a rectifying structure that allows for the system to begin operating [18,24,25]. Alternatively, individual transistors can be used to form active diode charge pumps [26,27] using the available bulk contact to form passive diodes for start-up. With a power consumption of ~5 μW this method is not well suited to low input power applications. However, charge pumps do offer some inherent advantages, especially in situations where boosting is necessary [5,22,26–29], because they can both cold-start and boost the voltage to a higher final value at the same time. Passive charge pumps are also a possibility. The disadvantage of passive charge pumps is that they exhibit very low efficiencies at low input voltages (<0.2 V_{AC}) due to the inability to overcome the Schottky diode turn-on voltages [5].

A simple method to overcome very low voltage inputs, one that is particularly suited toward electromagnetic harvesters, is to utilize transformers. They offer a passive way to overcome diode turn-on voltages. Additionally, high efficiencies (65%) have been demonstrated in transformer based systems [29–31] with low output impedances (3–4 Ω). It is essential that the output impedance of the harvester must be small, otherwise the size and power loss of the matched transformer would be impractical. Provided that the output impedance of the harvester is reduced in the PFIG, combining a passive charge pump with an input transformer can provide a simple and passive way of rectifying and boosting the output voltage of the PFIG. Additionally, for harvesters with two outputs (such as the PFIG), a passive charge pump can be used with one output to supply a high efficiency active rectifier that manages the other output [28].

This paper discusses the improved performance and robustness of the previously reported mechanical harvester PFIG-B1, including the adjustment of its technical characteristics with system level considerations in mind. With the new PFIG (PFIG-B2), a power management circuit consisting of input transformers and two cascaded passive charge pumps is used to rectify and boost the output voltage of the harvester and store energy on a capacitor. These enhancements allowed a complete system to be installed on a suspension bridge where it was monitored for 13 months, and its performance was remotely monitored and recorded starting April 30, 2012 [32]. Section 2 discusses the enhancements in the harvester and passive electronics. Section 3 discusses short-term system installations on the bridge, and Section 4 discusses the long-term system installations, and details how the system overcame the challenges presented in the introduction to obtain new understanding of the long-term PFIG performance.

2. Bridge harvesting system implementation

2.1. Harvester enhancements

The PFIG harvester has been further optimized to increase the output power and improve the long-term reliability. The PFIG architecture has been described in detail [5,13–15]. Changes implemented to maximize power transfer to the circuit include: decreasing the number of coil turns to lower the PFIG-B2's output impedance to 300 Ω; implementing a double magnet structure to better confine and route the flux; and changing the inertial mass suspension spring material to improve its reliability in combination with new assembly techniques.

Table 1
Summary of (PFIG and circuit) performance and characteristics.

Performance summary	
Minimum acceleration	0.34 m/s^2
Internal volume	43 cm^3
Total volume	68 cm^3
Avg. power (0.34 m/s^2, 2 Hz)	12.5 μW
Avg. power on New Carquinez Bridge	1.6–5.02 μW
Figure of merit, F_oM_v (0.34 m/s^2, 2 Hz)	0.16%
Altered mechanical parameters from previous PFIG [5]	
Coil turns (N)	1200
Coil resistance	275 kΩ
Spring constant, k_i (both springs combined)	535 N/m
Circuit characteristics	
Boosting methods	CW charge pump & transformer
Transformer	Picoelectronics T-22940
Transformer volume	5.09 cm^3
Diode	BAT54WS surface mount Schottky diode
Capacitors	10 μF (tantalum surface mount)
Maximum circuit efficiency	27%

The FIG output impedance was successfully reduced to 300 Ω in order to alleviate the challenges in the power management system resulting from a high impedance. At the same time, better positioning of the magnet relative to the coil increased the electromagnetic coupling. A second alternative was also explored whereby a double magnet structure using two oppositely poled magnets was implemented in order to confine the flux [33–35]. These changes provide more flux linkage and achieve a better volumetric efficiency in the FIG.

The spring suspension which carries the heavy central inertial mass was modified in this design. Previous experimentation with the PFIG-B1 harvester highlighted that this was a significant weak point in the device. More specifically, harvesters installed on infrastructure should be able to operate for many decades in order to produce value as compared to batteries. Therefore, future versions of the PFIG should be able to withstand stresses due to shipping, shock, and other short-term excitations in addition to being able to survive many decades of cyclical loading without undergoing fatigue. For this reason the material used in the PFIG-B2 was changed to stainless steel 17–7 rather than copper as before in the PFIG-B1; however, the spring constant was designed to remain the same at ~535 N/m (Table 1). Stainless steel has a hardness that is 11× that of copper. The springs were modified to have large curvature at the endpoints in order to minimize large stress concentrations resulting from abrupt edges and corners. Stresses can quickly build due to the large extension of the inertial mass spring, and repeated excessive stress can quickly lead to fatigue. The inertial mass suspension always has non-zero stress due to the displacement that gravity generates on the assembly. In addition to this, the bridge vibrations can produce additional displacement. For the purpose of simulation, COMSOL was used to examine the stress in the springs throughout the full motion range of the inertial mass (constrained by the FIGs which act as built in barriers to limit the deflection in case of excessive acceleration or shock). The results can be seen in Fig. 3. Of course, the highest stress is experienced at the fixed endpoints of each support arm. The von Mises stress (typically in the range of 0.5 to 0.7 GPa) is well below the yield strength of 1.3 GPa for the steel alloy that was used. Using standard cyclical fatigue theory [36] one can estimate that under these conditions the inertial mass suspension, the most critical part of the PFIG form a mechanical standpoint, can have a lifetime in the range of hundreds of years even at high frequency cycles of 50–100 Hz.

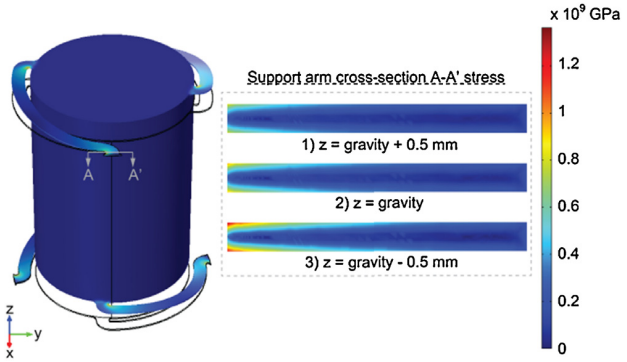

Fig. 3. Simulations in COMSOL show the von Mises stress experienced by the inertial mass suspension assembly under static gravitational loading as well as under applied bridge vibrations.

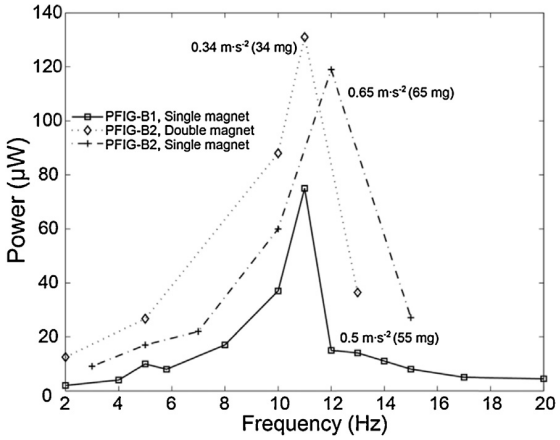

Fig. 4. The graph of frequency vs. power is shown for multiple versions of the PFIG. The enhanced PFIG-B2 with and without a double magnet structure show significantly improved power output as compared with the previous PFIG-B1.

Frequency vs. power plots for various versions of the PFIG are shown in Fig. 4. They are actuated at the minimum acceleration level needed for operation, which was designed to be different in each case in order to explore the limits of the harvester. The different acceleration levels in Fig. 4 should be considered when comparing the three plots. The highest output power in lab tests was achieved with the PFIG-B2 using two oppositely poled magnets. Without the double magnet structure, the PFIG-B2 still shows considerable improvement over previously reported results [5]. Lab testing of the PFIG-B2 (using the double magnet structure) produced 12.5 μW with an input sinusoidal acceleration of 0.34 m/s^2 and 2 Hz, which is a 7.5× improvement in Volume Figure of Merit, F_oM_v, to 0.16% [5]. Also, at 0.34 m/s^2 and 10 Hz, 88 μW of power was harvested with a F_oM_v of 0.22% [5] a 3× improvement over [5]. (The reported figures of merit in [5] are incorrect due to a calculation error. The actual F_oM_v at 2 Hz and 0.54 m/s^2 is 0.02% rather than 0.04% and the actual F_oM_v at 10 Hz and 0.54 m/s^2 is 0.073% rather than 0.17%.) While the double magnet structure showed better performance in the lab, as seen in Fig. 4, due to the tighter alignment tolerances and more complicated assembly, the single magnet arrangement was used in the long-term test discussed in Section 4.

2.2. Passive power management electronics

The PFIG-B1 used a cascade of two six-stage discrete charge pumps to boost and rectify the harvester output signal [5]. Schottky diodes (BAT54WS) were used in the charge pump. However, the diode drop losses significantly reduced both the efficiency and boosting ability of the previous circuit making it unsuitable for bridge operation. Therefore, any new interface has several requirements. First, the circuit must easily start-up based on the smallest expected harvester output. Next, the circuit should optimize power transfer to a load or storage capacitor at these very low harvester outputs. Finally, it should enable long-term installation of the bridge harvesting system (BHS), so that the limits of the system (PFIG and circuit) can be studied and characterized. To accomplish these goals and enable the rate at which the BHS storage capacitor rises to serve as the basis for estimating power during the bridge installation, the circuit needed to start-up and rapidly rise to a usable voltage from even the lowest PFIG output voltage signal (~60 mV). State-of-the-art ICs can regularly operate at 1.2–1.8 V, and there are even sub-threshold microcontrollers that can operate below 0.7 V. Because of this, the PFIG should be able to efficiently charge a storage capacitor to at least 0.7 V. Efficiency, η, is used to measure the performance of the circuit. Circuit efficiency is calculated in this case by comparing the average harvestable power that can be delivered to a matched resistive load (ideal case) to the power delivered by the power management circuit.

$$\eta = \frac{1/(t_2 - t_1)\int_{t1}^{t2} P_{\text{out-CW}}}{1/(t_2 - t_1)\int_{t1}^{t2} P_{\text{out-matched load}}} \quad (1)$$

Average output power can be measured in steady-state by loading the output with a resistor to obtain current and voltage. Alternately, average start-up output power can be obtained by measuring the energy in the storage capacitor divided by the storage period.

The addition of the transformers between the harvester and the charge pump immediately mitigates the effect of the diode turn-on voltage losses and even reduces the number of required multiplier stages while still significantly improving the circuit's boosting ability. Previously, for the circuit used with the PFIG-B1, without the addition of transformers and not taking into account the characteristic decay in the PFIG output waveform, the theoretically available maximum voltage of the cascaded charge pumps is $V_{\text{out}_{\text{CCW}}}$, where V_{CW} is the maximum output of a single Cockcroft–Walton multiplier:

$$V_{\text{out}_{\text{CCW}}} = 2 \times V_{\text{CW}} = 4 \times n \times V_{\text{Peak}} \quad (2)$$

here n is the number of stages per multiplier, and V_{Peak} is the unmatched input peak voltage. The factor of four comes from boosting the two serially cascaded Cockcroft–Walton multipliers. For the two six-stage cascaded multipliers the maximum boosting is:

$$V_{\text{out}_{\text{CCW}}} = 24 \times V_{\text{Peak}} \quad (3)$$

While this is significant boosting, the Schottky diode turn-on $V_{\text{diode-drop}}$ needs to be accounted for, resulting in the following:

$$V_{\text{out}_{\text{CCW}}} = 24 \times \left(V_{\text{Peak}} - V_{\text{diode-drop}}\right) \quad (4)$$

If the Schottky drop is near 180 mV, and the typical PFIG output maximum peak is 200 mV, most of the signal is wasted. This results in an output of 480 mV by using (4). Because the PFIG output decays, only the first few peaks will be useful and the rest of the output signal will be lost due to the diode drops. Ideally, the circuit would make use of as many of the decaying peaks as possible and be capable of operating from the low ~60 mV peaks.

The new circuit presented and used with the PFIG-B2 makes use of a transformer with a 1:10 multiplication factor to boost the low and decaying PFIG outputs. When the transformers are matched to the FIG output impedance, to obtain maximum power transfer, the voltage is reduced by a factor of two in essence resulting in

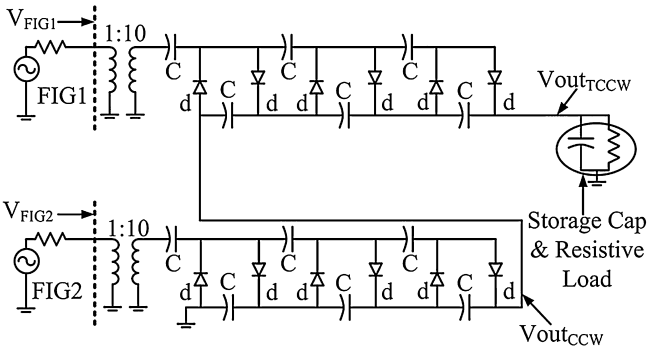

Fig. 5. The circuit schematic shows two transformers that increase the harvester outputs and feed them into two cascaded 3-stage Cockcroft–Walton Multipliers. The storage capacitor and load are indicated along with other important nodes [32].

a 5× gain in voltage. This gives the ideal maximum voltage for a circuit containing a Cockcroft-Walton Multiplier preceded by a 1:10 matched transformer as $V_{out_{TCCW}}$:

$$V_{out_{TCCW}} = 2 \times V_{CW} = 4 \times n \times \left(5 \times V_{Peak} - V_{diode\text{-}drop}\right) \quad (5)$$

Assuming $n = 3$ stages, a 180 mV diode turn-on voltage, and V_{Peak} of 60 mV, the boosted DC output is 1.44 V, which will yield ~0.72 V when optimally loaded. Therefore, the target requirements can be met with only 3 stages. The inter-stage capacitors were chosen to be 10 μF (Table 1) to quickly charge the charge pump while maintaining a reasonable efficiency.

The schematic of the interface circuit is shown in Fig. 5 and a photo of the realized circuit is shown in Fig. 6. The two transformers used in the system are Picoelectronics T-22490. Even at 200–300 Ω, the output impedance of each FIG still imposes stringent transformer characteristics. To maximize power transfer the transformer input impedance should match the impedance of the FIGs [37]. As discussed earlier, a transformer with a ratio of 1:10 was chosen. Higher ratios are possible; however, every additional turn added in a transformer increases its DC resistance. Producing a desired ratio and matched input impedance is a challenge. As part of the passive circuit design process, the efficiency of the matched T-22490 was measured to be ~63% with a 100 Hz signal and an input power of 6.4 μW. Picoelectronics transformers [38] are rated at 1 mW and have a frequency range of 20–25 kHz; however, at low frequency there seems to be significant reduction in

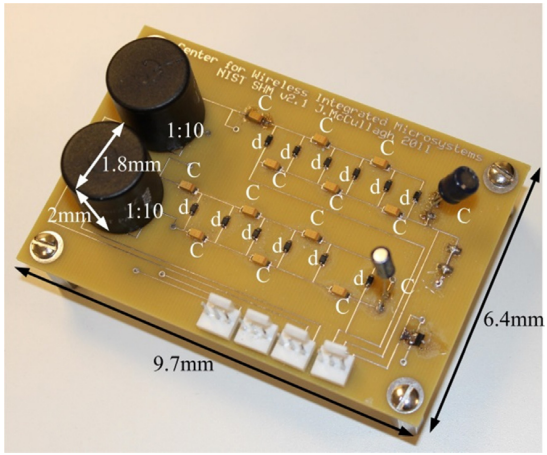

Fig. 6. The picture of the circuit used with two transformers and two cascaded Cockcroft–Walton multipliers. Capacitors, diodes and transformers are labeled C, d, and 1:10, respectively.

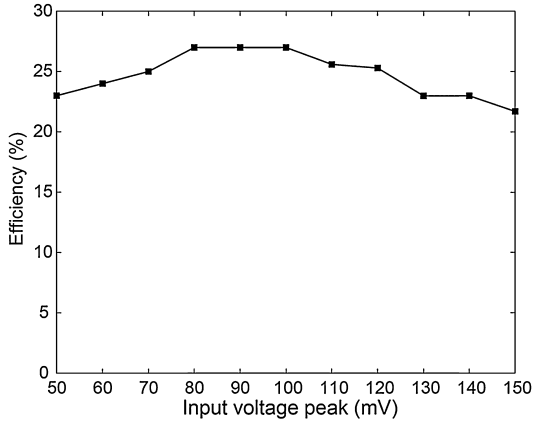

Fig. 7. Efficiency of the power management circuit using sinusoidal inputs at 130 Hz in place of FIGs (same output impedance). The output is held constant at 1.2 V by adjusting the output load. Both inputs are changed together to yield a maximum efficiency of 27%.

the inductive coupling. Laboratory measurements show that maximum efficiency occurs near 500 Hz, which is much higher than the frequency output of the FIGs (~130 Hz). The PFIG's 200 - 300 Ω impedance and the 1:10 multiplication factor result in a relatively large transformer. The diameter of the T-22490 is ~1.8 cm and the height ~2 cm resulting in a total volume of 5.09 cm^3, larger than the volume of each individual FIG.

The maximum circuit efficiency is measured using a 130 Hz sine-wave from a function generator with 300 Ω series resistances. The efficiency is 27%. Efficiencies up to 65% have been reported by others regarding other up-conversion works containing transformers [30,31]; however, these works have source impedances of 3–4 Ω. Because the efficiency of a rectifier changes as it charges a capacitor, the output is held constant at 1.2 V by varying the impedance, while the input voltage is varied. The results are shown in Fig. 7. Here the two charge pumps are cascaded and show a maximum efficiency of 27%. A half-wave multiplier only harvests the positive part of the input waveform reducing efficiency. Other efficiency losses are due to the transformers, diode drops, and loading between the cascaded charge pumps. Fig. 8 shows the efficiency of a single multiplier (including transformer). The maximum efficiency is 38%, which is higher than that obtained using cascading. Connecting the charge pumps together generates a higher output voltage, but charge coming from the bottom charge pump must again be boosted through

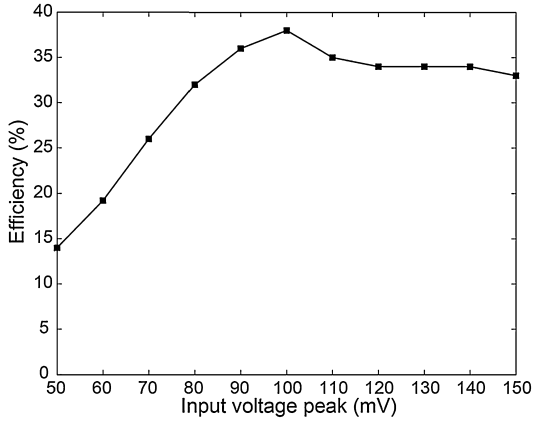

Fig. 8. Efficiency of a single Cockcroft–Walton 3-stage multiplier and transformer with a sinusoidal input at 130 Hz in place of FIGs (same output impedance). The output is held constant at 1.2 V by adjusting the output load. The input is changed to yield a max efficiency of 38%.

the top pump where it will face losses from another set of diode drops and leakage, thereby further reducing the circuit's overall efficiency.

To determine efficiency in a more realistic way, two function generators are used to approximate the PFIG outputs using two time-offset decaying sinusoids at 10 Hz. A very low input current op-amp (LMC6484, National Semiconductor) buffer is used to monitor the storage capacitor voltage. Holding the output constant at 1 V, by varying the output load, the efficiency was measured to be 14.4%. The measured efficiency of the circuit, charging a 10 μF capacitor from 0 to 0.7 V, is 5.5%. This efficiency is much lower than when the output is held constant. The reason for this is that the capacitors in the charge pump stages must be charged before optimal efficiency can occur at the output.

Table 2 compares the BHS system to other efforts aimed at mid to low frequency of both resonant and non-resonant signals. Low frequency (≤10 Hz) based harvesters [13,28–31,39] generally rely on frequency up-conversion, while higher frequency (≥10 Hz) based harvesters are generally resonant-based [40–47]. The ability of the BHS system to generate energy in extremely challenging conditions (combination of very low accelerations and frequency) is unrivalled. While the power management circuit efficiency still needs to be improved, the challenges in this application are more stringent than those previously faced by other works [28–31]. Clearly, further improving the harvester electromechanical transducers to produce higher voltage signals with a lower output impedance would greatly benefit the system's efficiency. However, other major works cited in Table 2 shows that an output impedance of 3–4 Ω is likely too low to be realistic for bridge harvesting applications. Another possibility for circuit improvement is that active rectification could be used to enhance the interface electronics.

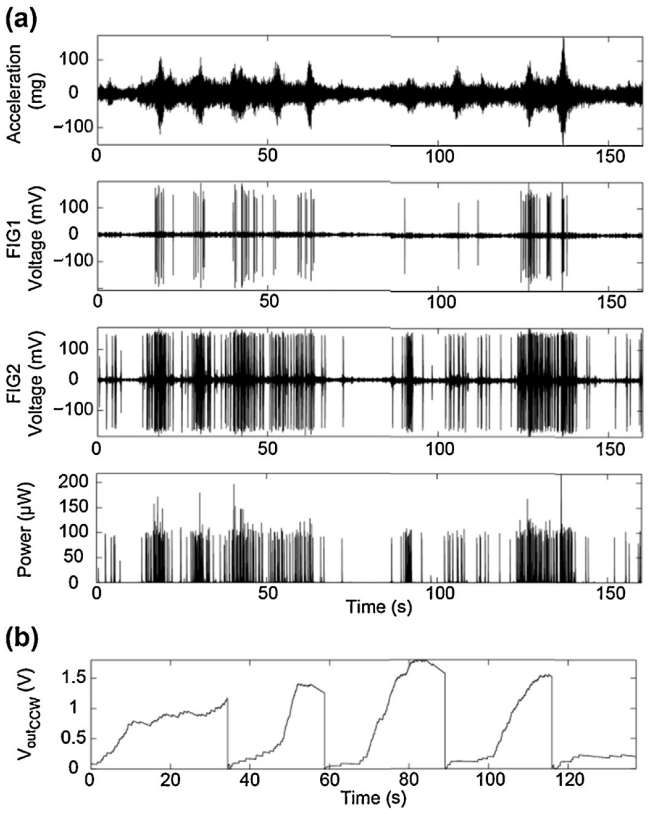

Fig. 9. (a) Short-term testing data showing acceleration, FIG1 and FIG2 outputs, and total instantaneous output power taken on the NCB; and (b) separately measured voltage on the storage capacitor taken at a different time than (a) [32].

3. On-site short term bridge tests

Two BHS units (containing the PFIG-B2 and passive electronics) were temporarily installed on the NCB for short-term tests. On-site testing allows for more detailed performance measurements to be made. An example of such an installation can be seen in Fig. 1a, where the harvester and an accelerometer are magnetically attached under the bridge. Initially, the harvester is tested using a matched load, and the signal is recorded with LabView. Sample waveforms are shown in Fig. 9a, where the average power produced is 3.24 μW. Small mismatches in the equilibrium positions of the two FIGs result in the asymmetric actuation. Table 3 shows the average power generated on the bridge at different locations. Two different versions of the PFIG-B2 were tested (with and without the double magnet structure). The best result in Table 3 is from location 2 where $P_{average}$ = 5.02 μW was generated over a time period of 125 s, and represents a 10× improvement over previously reported on-site testing results using the PFIG-B1 [5]. The double and single magnet structure gave similar results in the on-site bridge tests, while in the lab, the double magnet structure performed better (Fig. 4). There are two possible reasons for this. First, vibrations on the bridge can vary significantly from minute to minute, and the two PFIG designs were not tested at the same time. Second, the short-term tests were performed before design changes allowed for the harvester to be shipped fully assembled. This means that the harvester was assembled and adjusted on the bridge, resulting in only a rough optimization (much less accurate than a laboratory setting).

In a second set of experiments (Fig. 9b), the full BHS system (PFIG-B2 and circuit) was tested, and a 10 μF storage capacitor's voltage was repeatedly charged by the PFIG outputs and then manually discharged. The DC output could reach as high as 2 V within a reasonable time period (48 s); however, as seen in Fig. 9b, the higher the voltage, the slower the capacitor charges. At high output voltages, the lower voltage peaks of the decaying waveform are not harvested, while the highest peaks are harvested at a reduced efficiency. As the output voltage further increases, the peaks are no longer able to add any charge and so a maximum achievable voltage is reached. Additionally, there are parasitic leakage paths that limit the voltage, especially when the vibrations are sparse. The storage capacitor was continually discharged so an understanding of the rate at which the storage capacitor charges could be gained and used to optimize the system for the long-term installation discussed in the next section.

4. Long-term BHS testing

4.1. Long-term bridge test implementation

The goal was to install and monitor the BHS over a long period of time and to monitor the FIG outputs and the storage capacitor voltage, so that the BHS performance can be quantitatively assessed. For this goal a special-purpose *Narada* [2,15] wireless sensor node, already deployed on the NCB, is used. The *Narada* node samples the key BHS metrics once per hour for 90 s at a sampling rate of 100 Hz. The results are wirelessly transmitted to a base station and are then available through remote access [15]. To facilitate the long-term evaluation of the BHS, the *Narada* node automatically discharges the storage capacitor when it reaches 0.7 V. This allows for the average power to be estimated by the number of discharges in the 90-second sampling period. Solar cells on top of the bridge are wired and power the *Narada* node allowing it to perform the described functions. It is important to note that the BHS is not used to power the *Narada* wireless sensor node. Fig. 10a and

Table 2
Comparison of resonant, non-resonant, and selected circuit-focused harvester systems.

Harvester characteristics								Circuit characteristics			
Ref.	Harvester type	Volume (cm^3)	Acceleration (m/s^2)	Frequency (Hz)	Maximum power (μW)	F_oM_v (%)	Output R (Ω)	Boosting method	Maximum boosting	Start-up method	Max efficiency
[40]	EM resonant	1	–	110	830	0.10	1000	Charge pump	×4	Schottky diodes	–
[44]	EM resonant	0.15	8.829	60	0.586	0.018	110	–	–	–	–
[46]	EM resonant	0.15	0.59	52	46	24.88	4000	–	–	–	–
[47]	EM tunable	1.12	0.59	45	200	8.58	–	–	–	–	–
[41]	EM resonant	8.6	–	41	153	0.049	33	–	–	–	–
[42]	Coupled E&M -Piezo resonant	–	–	21.6	332	–	68 E&M 3500 Piezo	–	–	–	–
[43]	EM multiple resonances	27.38	9.8	10.3	5020	0.796	3000	–	–	–	–
[39]	Up conversion piezo free missile	25	–	10	600	0.003	400,000	–	–	–	–
[29,30]	EM up-conversion	2.96*	–	10	572	–	3–4	Charge pump/rectifier/transformer	×15	Discrete device diode	35%
[30,31]	EM up-conversion	2.96*	–	10	572	–	3–4	Transformer/rectifier	×10	IC rectifier (*V*th dependent)	65%
[28]	Up-conversion/EM free magnet	16	10.1	8	97	0.039	27.5/55	Charge pump/active rectifier	×2	IC rectifier (*V*th dependent)	80% (only 1 of 2 coils)
[7]	EM resonant	18.1	1	4.1	980	6.63	290	–	–	–	–
[5]	PFIG EM	43	0.54	10	57	0.073	1500	Charge pump	×24	Schottky diodes	12%
		43	0.54	2	2.3	0.02	1500				
This Work	PFIG	43	0.34	10	88	0.22	275	Charge pump/transformer	×60	Schottky diodes	27% (14.4% decaying)
	EM	43	0.34	2	12.5	0.16	275				
Selected circuit-focused work											
[20]	EM	–	–	10,000	–	–	–	Rectifier	×1	Passive rectifier	90%
[25]	Piezo	–	9.8	3900	–	–	11,000–350,000	Rectifier/LC boost	∼×3	Passive rectifier	79%
[21]	Piezo multiple resonances	–	–	1035	38	–	–	Multiple input rectifiers	×1	IC rectifier (*V*th dependent)	98.3%
[23]	Piezo with feedback	0.23	–	100	72	–	5000,000	LC boost	×3.5	Pre-charged	49.9%
[18]	EM	–	–	50	40	–	2043	Switched cap charge pump	×3.5	Pre-charged	50%
[22]	EM	–	–	44	900	–	80	LC boost	∼×12	Passive charge pump	76%

* Not self-contained.

Table 3
Short-term results for double and single magnet PFIG designs at different bridge locations.

Location (Fig. 1)	Average power, PFIG (double magnet) (μW)	Average power, PFIG (single magnet) (μW)
1	4.4	3.24
2	3.13	5.02
3	3.73	–
4	1.6	–

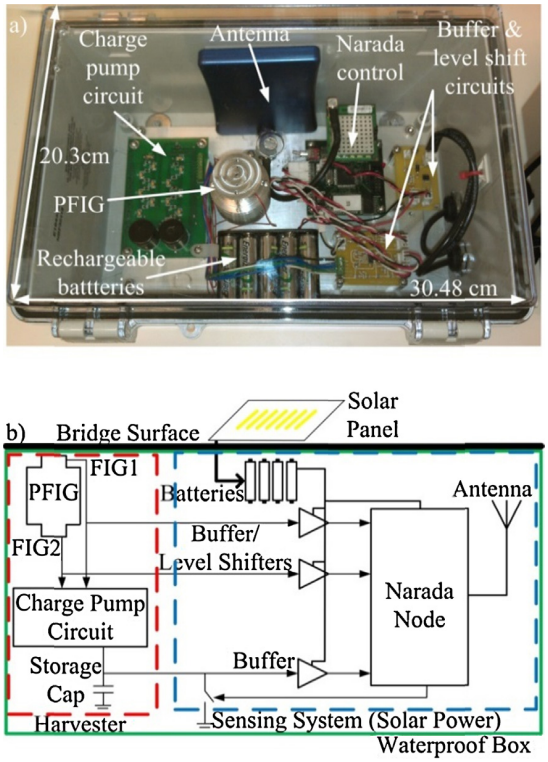

Fig. 10. The PFIG, passive harvesting circuit, *Narada* control, *Narada* antenna, buffer and level shift circuits used in the long-term test on the New Carquinez Bridge. (a) The water tight box and (b) a schematic of the long-term test system [32].

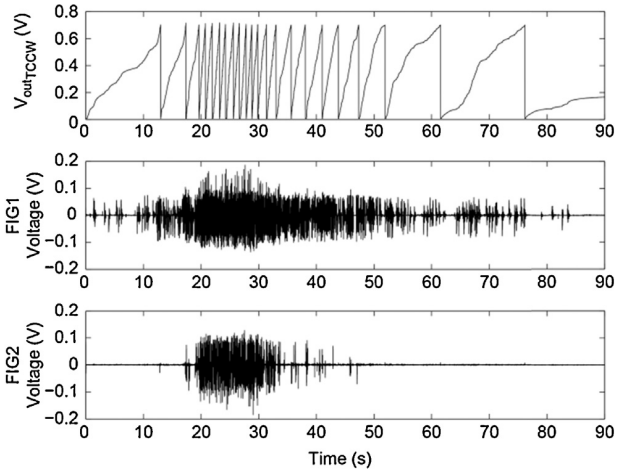

Fig. 11. Data recorded on May 29, 2012 by the *Narada* wireless node [32].

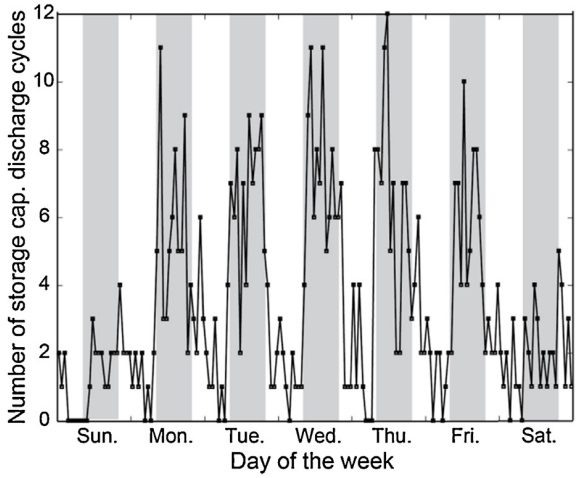

Fig. 12. Circuit discharges for one week starting May 13, 2012. Each circuit discharges represents approximately 0.5 μW in unprocessed PFIG output power. The shaded areas represent 8 am to 8 pm [32].

b shows the long-term test system. The PFIG, harvesting circuit, buffer and level shift circuits, transmission antenna, *Narada* node, and rechargeable batteries (powered by solar panels on top of the bridge) are contained inside a commercially available water-tight box. The batteries are used to power the *Narada* system, the buffers, and the level-shift circuits, which interface the BHS to the *Narada* node. The dimensions of the box are 30.5 × 20.3 × 13.2 cm. On April 30, 2012, two of these water tight boxes were installed under the bridge deck at location 1 (Fig. 1b).

4.2. Results

A sample of recorded data is shown in Fig. 11. The voltage on the storage capacitor rises faster and is discharged more frequently when the FIGs actuate more often and at higher amplitudes. The FIG outputs are under-sampled at 100 Hz (sample rate chosen to minimize *Narada* power consumption). Nonetheless, the basic functionality of the system can be discerned from the plots.

Fig. 12 summarizes one week of data. Harvested power is greater during daytime and weekdays. Each discharge occurring at 0.7 V on the 10 μF capacitor, recorded during a 90 s period, corresponds to 27 nW of power delivered to a load. Once again, it should be noted that data recordings are only made once per hour and the number of discharges shown in Fig. 12 is only during the several 90 s measurement windows. Lab measurements described earlier estimated the efficiency of the PFIG and circuit during start-up to be 5.5%. Therefore, each capacitor discharge corresponds to an unprocessed PFIG output power of ~0.5 μW, and the results in Fig. 12 indicate a nearly identical amount of power harvested during daytime (2–12 discharges or 1.0–6.0 μW) as was measured during the short-term tests of the PFIG (Table 1). Fig. 13 further verifies these power levels. It shows a histogram of the number of discharges in a 90 s period from May 1st to June 18th in 2012. Fig. 13 shows the histogram peak centers around 1 and 2 discharges, with 0 to 11 discharges being common. The mean and median of the data in Fig. 13 is 3.29 discharges and 3 discharges. As each discharge represents approximately 0.5 μW produced by the PFIG, it can be concluded that for an optimally functioning PFIG, average power in the range of 1.5 μW to 2 μW is common, going up to 3 μW during daytime.

The BHS has operated continuously on the NCB for 13 months starting April 30, 2012 (Fig. 14). Starting in late October 2012, the wireless data collection system began to have outages. In many of these cases, measurements from the BHS locally written to non-volatile memory on the wireless sensor node were still received a few times a day. The root cause of this is suspected to be the solar harvesting used to power the *Narada* nodes. Likely, there was not

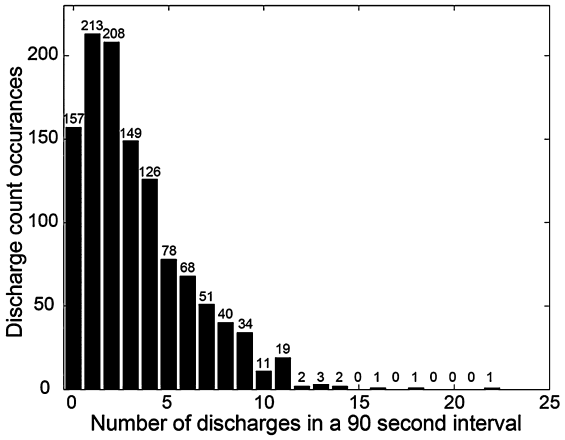

Fig. 13. A histogram of the discharge counts per 90 s period. Data from May 1st–June 18th is shown. The median value is 3 while the mean value is 3.29. The specific discharge count occurrence frequency is shown above the histogram bar.

enough light during this time of the year (winter season) when wet and foggy weather is common. This highlights a potential weakness of solar energy harvesting in unmanned systems. In the long-term test (Fig. 14), the same weekly pattern seen in Fig. 12 continues to be observed, as well as sharp drops in harvested power on U.S. national holidays. Over the first six weeks the power output remained relatively consistent. The highest power was recorded the morning following Memorial Day on May 29th, 2012 and is estimated to be 10.9 μW (22 discharges over 90 s, Fig. 14). The data clearly demonstrates that the power harvested correlates directly to traffic and thus could be a sensed variable itself. The PFIG exhibited a reduction in power at the end of June 2012, producing approximately half as much energy. The mechanism for such a decrease will be discussed next.

4.3. Long-term performance discussion

The results in Fig. 14 show a significant reduction in performance after six weeks in mid-June 2012. The system was retrieved on January 28, 2014 to understand the root cause of this power decrease and to understand the system's general health after over one year of testing starting April 30, 2012. After 13 months there was a significant loss of monitoring data. It was discovered upon retrieval that the PFIG and interface electronics remained functional; however, the loss of data occurred because the rechargeable batteries powering the wireless sensor had weakened preventing reliable wireless communications. Energizer AA 2300 mA h rechargeable batteries (NH15-2300) were used with a ~1.3 V maximum voltage. The last month of operation in Fig. 14 is marked as grey because the monitoring system was never operational for an entire day, and only ~1/5th of the set of 90 s measurements was completed. The *Narada* system uses a linear regulator (LP2986 Texas Instruments) with an input of ~60 mA at >6.0 V achieved with five batteries in series. A low voltage cutoff circuit turns the system off when the batteries drop to 5.7 V to maintain *Narada* functionality. It is suspected that a decrease in recharge battery capacity lowered the maximum battery voltage. This lowered battery voltage frequently fell below the linear regulator cutoff resulting in a less reliable wireless sensor for long-term field operation. To avoid the inherent lifetime limitations with batteries, future long-term harvesting designs will likely use ultracapacitors to improve storage lifetime to decades of use.

In the retrieved system, the PFIG inertial mass springs were not deformed and the electronics remained functional, but the bottom set screw of the system was loose. The schematic of the PFIG, Fig. 2, shows that for the ease of assembly the individual FIGs are held in place only by the friction of set screws along the side of the FIG casing as well as one on the bottom. This makes this assembly method susceptible to slipping, especially when the bottom set screw was loosened because nothing stops the vertical slippage of the FIG. A study of frequency versus power, similar to Fig. 4, was completed on the retrieved PFIG. Resonance remained the same at ~12 Hz, meaning the spring constant remained unchanged at 535 N/m as expected. At lower frequencies (<9 Hz) the minimum acceleration necessary for actuation of both FIGs decreased to 80–100 mg. This would explain the 2/3 power decrease seen in Fig. 14.

A wide range of frequencies and amplitudes are exhibited on the bridge, the response of the inertial mass-spring system can be unpredictable. It can be driven into resonance at its natural frequency around 10–12 Hz, and at high amplitudes it can begin to strike the top of the FIG casing, which also serves as a safety barrier to protect the internal mechanism. Experimental results in both the laboratory and during the short-term tests have shown that striking the end-stops can drive the inertial mass system into a non-linear regime that can even amplify the amplitude of the motion. In the laboratory, we have verified that repeated contact between the inertial mass and the FIG surface produces enough force to decrease the PFIG performance even when the set screws were securely tightened before the experiment. By readjusting the FIG positions, the performance loss can be regained. Similar to previous PFIG versions [13,14], Matlab-based simulation analysis of the PFIG-B2 shows that a ~10–40 micrometers slip in FIG position can change minimum acceleration by ~2–10 mg at lower

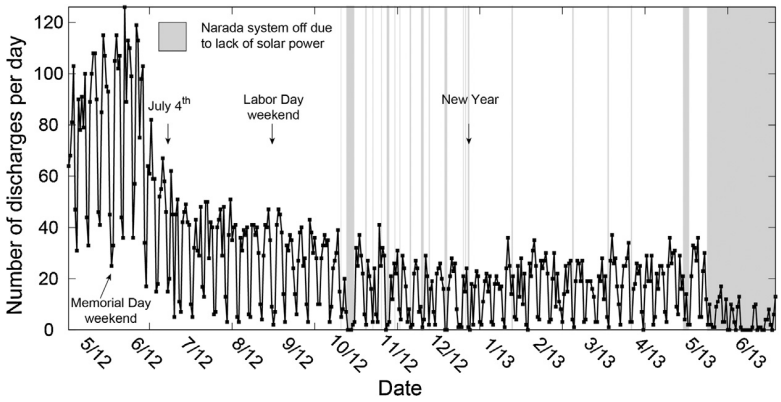

Fig. 14. Entire transmitted data set since installation on April 30, 2012. Each point represents the total number of discharges per day over 24 ninety-second recording periods. Grey areas represent periods where the *Narada* system was not functional due to solar panels not collecting power.

frequencies (<5 Hz). This slippage explains the decrease in power over time shown in Fig. 14.

The set-screws were included to allow for different experiments to be carried out in the lab by varying the FIG positions, prior to PFIG-B2 installation on the bridge. In the future the set-screws will be removed and the FIG position will be fixed in place within the harvester mechanism. In the broad area of vibration harvesters and frequency up-converting harvesters such as the PFIG, analysis has been done on what environmental conditions can potentially cause harvester failure [48]. Usually this analysis focuses on damage that can be caused by a single shock to the system that can physically break the system; however, failure mechanisms such as FIG slippage mean that the damage can be gradual, and the harvester may still be functional even after damage has occurred.

5. Conclusion

This paper discusses the development and long-term testing of a bridge harvesting system (BHS), including improvements in the vibration harvester and its power management circuitry with the goal of providing power for structural health monitoring. The short-term and long-term testing of the BHS on the New Carquinez suspension bridge shows a 10× improvement in unprocessed harvested power (PFIG-B2) [32] compared to a previous version (PFIG-B1) [5]. A new power management circuit is presented, which can "cold-start" without any pre-charged voltage and can boost the very low-voltage and decaying PFIG signal. By using a transformer followed by a charge pump, a 10 μF capacitor can charge up to 2 V on the bridge. The average unprocessed PFIG power is between 1 μW and 6 μW, while the maximum observed power is estimated to be 10.9 μW. The long-term study showed a decrease in harvested power after approximately six weeks. The cause of this reduced power is slippage of the FIG position, which has been repeated in the lab and verified with the retrieved harvester. It can be eliminated in future harvester designs. The circuit efficiency of 14.4% allows for a 10 μF capacitor to quickly charge to a high voltage based on the low voltage PFIG inputs allowing for the circuit's use in the long-term test. This circuit provides a proof-of-concept design with efficiency that can readily be improved by using active circuits designed in a low-power IC technology and by eliminating the transformers. Without the use of transformers in the circuit interface, the PFIG can be optimized for power without taking the output impedance into account.

The most unique result is that the BHS system was continuously functional and monitored for more than one year on the New Carquinez Bridge in California. The combination of harvester and electronics improvements allowed the system to function for over a year and were it not for the malfunctioned rechargeable battery of the wireless sensor, the system could have continued to operate while being monitored for even longer. Nevertheless, this 13-month study provided further understanding of the PFIG's long-term performance capabilities, and the lessons learned will motivate further improvements in future PFIG research. Energy harvesting applications derive their value from the ability to operate for many years and decades, and this is the first published long-term study of a mechanical harvester and system.

Acknowledgements

The authors thank Dr. Masahiro Kurata (Kyoto University) and Mr. Ed Thometz (California Department of Transportation) for invaluable assistance during bridge visits. This work is supported by the National Institute of Standards and Technology (NIST) Technology Innovation Program (TIP) under Cooperative Agreement Number 70NANB9H9008.

References

[1] US Department of Transportation, Our Nation's Highways: 2011, October, 2012, ⟨http://www.fhwa.dot.gov/policyinformation/pubs/hf/pl11028/chapter7.cfm#fig72⟩.
[2] M. Kurata, J. Lynch, G. van der Linden, V. Jacob, P. Hipley, Preliminary study of a wireless structural monitoring system for the New Carquinez Suspension Bridge, in: Proceedings of the Fifth World Conference on Structural Control and Monitoring, 2010, pp. 1–14.
[3] K.M. Farinholt, N. Miller, W. Sifuentes, J. MacDonald, G. Park, C.R. Farrar, Energy harvesting and wireless energy transmission for embedded SHM sensor nodes, Struct. Health Monit. 9 (2010) 269.
[4] T. Galchev, J. McCullagh, R.L. Peterson, K. Najafi, A. Mortazawi, Energy harvesting of radio frequency and vibration energy to enable wireless sensor monitoring of civil infrastructure, in: SPIE Smart Structures and Materials + Nondestructive Evaluation and Health Monitoring, 2011, pp. 798314–1798314.
[5] T. Galchev, J. McCullagh, R. Peterson, K. Najafi, Harvesting traffic-induced vibrations for structural health monitoring of bridges, J. Micromech. Microeng. 21 (2011) 1–13.
[6] E. Sazonov, L. Haodong, D. Curry, P. Pillay, Self-powered sensors for monitoring of highway bridges, IEEE Sens. J. 9 (2009) 1422–1429.
[7] S.-D. Kwon, J. Park, K. Law, Electromagnetic energy harvester with repulsively stacked multilayer magnets for low frequency vibrations, Smart Mater. Struct. 22 (2013) 055007.
[8] M. Peigney, D. Siegert, Piezoelectric energy harvesting from traffic-induced bridge vibrations, Smart Mater. Struct. 22 (2013) 095019.
[9] C. Eichhorn, R. Tchagsim, N. Wilhelm, P. Woias, A smart and self-sufficient frequency tunable vibration energy harvester, J. Micromech. Microeng. 21 (2011) 1–11.
[10] S. Roundy, Y. Zhang, Toward self-tuning adaptive vibration-based microgenerators, in: Smart Materials, Nano-, and Micro-Smart Systems, 2005, pp. 373–384.
[11] H. Kulah, K. Najafi, Energy scavenging from low-frequency vibrations by using frequency up-conversion for wireless sensor applications, IEEE Sens. J. 8 (2008) 261–268.
[12] T. Galchev, H. Kim, K. Najafi, Non-resonant bi-stable frequency-increased power scavenger from low-frequency ambient vibration, Solid-State Sensors, Actuators and Microsystems Conference, 2009. Transducers 2009. International (2009) 632–635.
[13] T. Galchev, H. Kim, K. Najafi, Micro power generator for harvesting low-frequency and nonperiodic vibrations, J. Microelectromech. Syst. 20 (2011) 852–866.
[14] T. Galchev, E.E. Aktakka, K. Najafi, A piezoelectric parametric frequency increased generator for harvesting low-frequency vibrations, J. Microelectromech. Syst. 21 (2012) 1311–1320.
[15] M. Kurata, J.P. Lynch, T. Galchev, M. Flynn, P. Hipley, V. Jacob, G. Van der Linden, A. Mortazawi, K. Najafi, R.L. Peterson, A two-tiered self-powered wireless monitoring system architecture for bridge health management, in: SPIE Smart Structures and Materials, San Diego, CA, 2010.
[16] E.E. Aktakka, R.L. Peterson, K. Najafi, A self-supplied inertial piezoelectric energy harvester with power-management IC, 2011 IEEE International Solid-State Circuits Conference Digest of Technical Papers (ISSCC) (2011) 120–121.
[17] H. Ulusan, K. Gharehbaghi, O. Zorlu, A. Muhtaroglu, H. Kulah, An efficient integrated interface electronics for electromagnetic energy harvesting from low voltage sources, in: 17th International Solid-State Sensors Actuators and Microsystems Conference (Transducers), Barcelona, Spain, 2013, pp. 450–453.
[18] D. Maurath, P.F. Becker, D. Spreemann, Y. Manoli, Efficient energy harvesting with electromagnetic energy transducers using active low-voltage rectification and maximum power point tracking, IEEE J. Solid-State Circuits 47 (2012) 1369–1380.
[19] C. Peters, D. Spreemann, M. Ortmanns, Y. Manoli, A CMOS integrated voltage and power efficient AC/DC converter for energy harvesting applications, J. Micromech. Microeng. 18 (2008) 104005.
[20] C. Peters, J. Handwerker, D. Maurath, Y. Manoli, A sub-500 mV highly efficient active rectifier for energy harvesting applications, IEEE Transactions on Circuits and Systems I: Regular Papers 58 (2011) 1542–1550.
[21] N.J. Guilar, R. Amirtharajah, P.J. Hurst, A full-wave rectifier with integrated peak selection for multiple electrode piezoelectric energy harvesters, IEEE J. Solid-State Circuits 44 (2009) 240–246.
[22] G.D. Szarka, S.G. Burrow, B.H. Stark, Ultralow power, fully autonomous boost rectifier for electromagnetic energy harvesters, Trans. IEEE Power Electron. 28 (2013) 3353–3362.
[23] K. Dongwon, G.A. Rincon-Mora, A single-inductor AC–DC piezoelectric energy-harvester/battery-charger IC converting ±(0.35 to 1.2 V) to (2.7 to 4.5 V), Solid-State Circuits Conference Digest of Technical Papers (ISSCC), 2010 IEEE International (2010) 494–495.
[24] C. Shuo, J. Ying, R. Yuan, D.P. Arnold, An active voltage doubling AC/DC converter for low-voltage energy harvesting applications, IEEE Trans. Power Electron. 26 (2011) 2258–2265.
[25] S. Bandyopadhyay, A.P. Chandrakasan, Platform architecture for solar, thermal, and vibration energy combining with MPPT and single inductor, IEEE J. Solid-State Circuits (2012) 1–17.

[26] C. Shuo, R. Sathe, R.D. Natarajan, D.P. Arnold, A voltage-multiplying self-powered AC/DC converter with 0.35 V minimum input voltage for energy harvesting applications, 2011 Twenty-Sixth Annual IEEE Applied Power Electronics Conference and Exposition (APEC) (2011) 1311–1318.
[27] S. Harrasi, A.S. Holmes, Synchronous voltage doubler for electromagnetic harvesters, in: PowerMEMS, Atlanta, GA, 2012, pp. 68–71.
[28] A. Rahimi, O. Zorlu, A. Muhtaroglu, H. Kulah, Fully self-powered electromagnetic energy harvesting system with highly efficient dual rail output, IEEE Sens. J. 12 (2012) 2287–2298.
[29] A. Rahimi, O. Zorlu, H. Kulah, A. Muhtaroglu, An interface circuit prototype for a vibration-based electromagnetic energy harvester, 2010 International Conference on Energy Aware Computing (ICEAC) (2010) 1–4.
[30] O. Zorlu, E.T. Topal, H. Kulah, A vibration-based electromagnetic energy harvester using mechanical frequency up-conversion method, IEEE Sens. J. 11 (2011) 481–488.
[31] A. Rahimi, O. Zorlu, A. Muhtaroglu, H. Kulah, A vibration-based electromagnetic energy harvester system with highly efficient interface electronics, 2011 16th International Solid-State Sensors Actuators and Microsystems Conference (Transducers) (2011) 2650–2653.
[32] J. McCullagh, R.L. Peterson, T. Galchev, R. Gordenker, Y. Zhang, J. Lynch, K. Najafi, Short-term and long-term testing of a vibration harvesting system for bridge health monitoring, in: PowerMEMS, Atlanta, GA, 2012, pp. 109–112.
[33] S. Cheng, D.P. Arnold, A study of a multi-pole magnetic generator for low-frequency vibrational energy harvesting, J. Micromech. Microeng. 20 (2010) 025015.
[34] T. von Büren, G. Tröster, Design and optimization of a linear vibration-driven electromagnetic micro-power generator, Sens. Actuators, A: Phys. 135 (2007) 765–775.
[35] A. Munaz, G.S. Chung, Design fabrication and characterization of a vibration driven electromagnetic energy harvester based on multi-pole magnet, in: PowerMEMS, Seoul, Republic of Korea, 2011.
[36] J. Bannantine, J. Comer, J. Handrock, Fundamentals of Metal Fatigue Analysis, first ed., Prentice-Hall, Inc., Englewood Cliffs, NJ, 1990, pp. 1–87.
[37] N. Mohan, T. Undeland, W. Robbins, in: B. Zobrist, C. Cervoni (Eds.), Power Electronics, third ed., John Wiley & Sons, Inc., Hoboken, NJ, 2003, pp. 52–56.
[38] Picoelectronics, Picoelectronics: Ultra Miniature Transformers, T Series Plug-In, April, 2013, ⟨http://www.picoelectronics.com/plugin/pe42_43.htm⟩.
[39] M. Renaud, P. Fiorini, R. van Schaijk, C. Van Hoof, Harvesting energy from the motion of human limbs: the design and analysis of an impact-based piezoelectric generator, Smart Mater. Struct. 18 (2009) 035001.
[40] N.N. Ching, H. Wong, W.J. Li, P.H. Leong, Z. Wen, A laser-micromachined multi-modal resonating power transducer for wireless sensing systems, Sens. Actuators, A: Phys. 97 (2002) 685–690.
[41] E. Sardini, M. Serpelloni, An efficient electromagnetic power harvesting device for low-frequency applications, Sens. Actuators, A: Phys. 172 (2011) 475–482.
[42] V.R. Challa, M. Prasad, F.T. Fisher, A coupled piezoelectric–electromagnetic energy harvesting technique for achieving increased power output through damping matching, Smart Mater. Struct. 18 (2009) 095029.
[43] K. Ashraf, M. Khir, J. Dennis, Z. Baharudin, Improved energy harvesting from low frequency vibrations by resonance amplification at multiple frequencies, Sens. Actuators, A: Phys. (2013) 123–132.
[44] S. Kulkarni, E. Koukharenko, R. Torah, J. Tudor, S. Beeby, T. O'Donnell, S. Roy, Design, fabrication and test of integrated micro-scale vibration-based electromagnetic generator, Sens. Actuators, A: Phys. 145 (2008) 336–342.
[45] D. Zhu, S. Beeby, J. Tudor, N. Harris, Vibration energy harvesting using the Halbach array, Smart Mater. Struct. 21 (2012) 075020.
[46] S.P. Beeby, R. Torah, M. Tudor, P. Glynne-Jones, T. O'Donnell, C. Saha, S. Roy, A micro electromagnetic generator for vibration energy harvesting, J. Micromech. Microeng. 17 (2007) 1257.
[47] I.N. Ayala, D. Zhu, M.J. Tudor, S.P. Beeby, Autonomous tunable energy harvester, PowerMEMS (2009) 49–52.
[48] R. St. Pierre, C. Livermore, Coupled-motion harvesting vs. plucked harvesting: which performs better? in: PowerMEMS, Atlanta, GA, 2012, pp. 207–210.

Biographies

James McCullagh is a Research Fellow in the Department of Civil and Environmental Engineering at the University of Michigan. Dr. McCullagh received his PhD in Electrical Engineering at the University of Michigan (2014), his M.S. at Purdue University in Electrical Engineering (2001) and his bachelor's degree in Physics at Carleton College (1998). He worked for 7 years in industry for IBM, JDS Uniphase, and Hitachi (HGST) as an analog IC designer and integration engineer. He is a recipient of the GAANN national fellowship and won a "Best Student Paper Award" at PowerMEMs 2012 in Atlanta Ga. His interests include vibration harvesting, power electronics, and low power IC design.

Tzeno Galchev received B.S. degrees in both Electrical and Computer Engineering in 2004, and M.S. and Ph.D. degrees in Electrical Engineering in 2006 and 2010 respectively, all from the University of Michigan, Ann Arbor. He is currently a Marie Curie Research Fellow in the Department of Microsystems Engineering (IMTEK) at the University of Freiburg in Germany. His research interests lie in the development of autonomous microsystems including the development of energy harvesting devices, sensors, actuators, analog and digital integrated circuits, and microfabrication and packaging technologies. Dr. Galchev was the sole recipient of the University of Michigan Excellence in Engineering Fellowship in 2006, he was awarded the John Atanasoff Certificate in 2008 by the President of Bulgaria for significant contributions in the development of information technologies by young scientists, Alexander von Humboldt Fellowship in 2011, and a Marie Curie Fellowship in 2013.

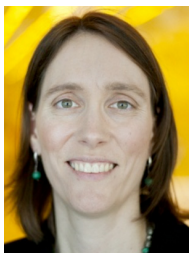

Rebecca L. (Becky) Peterson is an Assistant Professor of Electrical Engineering and Computer Science at the University of Michigan. Dr. Peterson received her PhD at Princeton University, her M.S. at University of Minnesota, and her B.S. at University of Rochester, NY, all in Electrical Engineering. She previously was a post-doctoral researcher at the Cavendish Laboratory and an Associate Lecturer in Engineering at Newnham College, both at the University of Cambridge. Her current research topics include solution processed electronic materials, novel devices using amorphous oxide semiconductors, and their additive hetero-integration with CMOS and MEMS. She is a recipient of a 2014 DARPA Young Faculty Award, and an NSF Graduate Research Fellowship.

Robert J.M. Gordenker received the B.S degree in electrical engineering from the University of Michigan in 1994. Since 2000 he has been on the technical staff for the research groups of Prof. Kensall Wise and Prof. Khalil Najafi at the University of Michigan. From 2006-2011 he served as the Technical Director for the NSF Engineering Research Center for Wireless Integrated MicroSystems (WIMS). Since 2012 his focus has been on providing technical advice, instrumentation and managing the test facilities for Prof. K. Najafi's research group. Prior to joining the University of Michigan, Mr. Gordenker was a member of the team which founded Irwin Magnetics (Ann Arbor, MI), where he held technical and management positions in Test Engineering and Operations. He was also a member of the team which turned around Applied Intelligent Systems (Ann Arbor, MI), with positions in Product Development, Operations and Reliability Engineering.

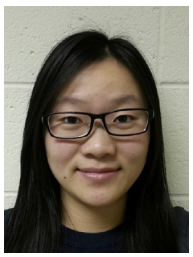

Yilan Zhang is a doctoral student in Civil and Environmental Engineering at the University of Michigan. She is also a master's student in Computer Science and Engineering. Yilan completed her B.S.E. and M.S.E degree in Civil and Environmental Engineering at the University of Michigan in 2011 and 2012. Her current research interests are in cyberinfrastructure for structural monitoring systems, long-term large-scale wireless structural monitoring, and data driven analytics for damage detection and decision making.

Jerome Lynch is a Professor of Civil and Environmental Engineering at the University of Michigan; he is also a faculty member with the Department of Electrical Engineering and Computer Science. Dr. Lynch completed his graduate studies at Stanford University where he received his PhD in Civil and Environmental Engineering in 2002, MS in Civil and Environmental Engineering in 1998, and MS in Electrical Engineering in 2003. His current research interests are in the areas of wireless structural monitoring, feedback control, and damage detection algorithms. Dr. Lynch was awarded the 2005 Office of Naval Research Young Investigator Award, the 2007 University of Michigan Henry Russel Award, the 2008 College of Engineering (University of Michigan) 1938E Award, and the 2009 Presidential Early Career Award for Scientists and Engineers by the U.S. White House.

Khalil Najafi is the Schlumberger Professor of Engineering, and Chair of Electrical and Computer Engineering at the University of Michigan since September 2008. He served as the Director of the Solid-State Electronics Laboratory from 1998-2005, the deputy director of the NSF ERC on Wireless Integrated Microsystems (WIMS) from 2000-2009, and has been the director of NSF's National Nanotechnology Infrastructure Network (NNIN) since 2004. He received the B.S., M.S., and the Ph.D. degrees in 1980, 1981, and 1986 respectively, all in Electrical Engineering from the University of Michigan, Ann Arbor. His research interests include: micromachining technologies, micromachined sensors, actuators, and MEMS; analog integrated circuits; implantable biomedical microsystems; hermetic and vacuum packaging; and low-power wireless sensing/actuating systems; inertial sensing systems.

Dr. Najafi has been active in the field of solid-state sensors and actuators for thirty years. He has been involved in several conferences and workshops dealing with micro sensors, actuators, and microsystems, including the International Conference on Solid-State Sensors, Actuators, and Microsystems, the Int. IEEE Micro-Electro-Mechanical Systems (MEMS) Conference, and the Hilton-Head Solid-State Sensors, Actuators and Microsystems Workshop. He has served as associate editor or editor of several journals, including IEEE Trans. Electron Devices, IEEE J. Solid-State Circuits, IEEE J. Micro-Electro-Mechanical-Systems (JMEMS), IEEE Trans. On Biomedical Engineering, IOP J. Micromechanics and Microengineering, Sensors and Materials, and Biomedical Microdevices. He currently serves on the editorial board of the IEEE Proceedings. He is a Fellow of the IEEE and the AIBME.